VII International Conference on Computational Methods for Coupled Problems in Science and Engineering
COUPLED PROBLEMS 2017
M. Papadrakakis, E. Oñate and B. Schrefler (Eds)

# MODELING OF AN ELECTRICALLY DRIVEN DROPLET GENERATOR

**YUN OUEDRAOGO*, ERION GJONAJ*, THOMAS WEILAND*, HERBERT DE GERSEM*, CHRISTOPH STEINHAUSEN†, GRAZIA LAMANNA†, BERNHARD WEIGAND†, ANDREAS PREUSCHE‡ AND ANDREAS DREIZLER‡**

*Institut für Theorie Elektromagnetischer Felder
Technische Universität Darmstadt
Schloßgartenstr. 8, 64289 Darmstadt, Germany
email: {ouedraogo,gjonaj,thomas.weiland,degersem}@temf.tu-darmstadt.de

†Institut für Thermodynamik der Luft- und Raumfahrt
Universität Stuttgart
Pfaffenwaldring 31, 70569 Stuttgart, Germany
email: {christoph.steinhausen,grazia.lamanna,bernhard.weigand}@itlr.uni-stuttgart.de

‡Fachgebiet für Reaktive Strömungen und Messtechnik
Technische Universität Darmstadt
Jovanka-Bontschits-Str. 2, 64287 Darmstadt
email: {preusche,dreizler}@rsm.tu-darmstadt.de

**Key words:** Electrohydrodynamics, On-demand droplet, Multiphase flow, VOF

**Abstract.** An electrohydrodynamic model for the simulation of droplet formation, motion and detachment in an electrically driven droplet generator is introduced. The numerical approch is based on the coupled solution of the multiphase flow problem with the charge continuity equation. A conduction-convection model, taking into account conductive, capacitive and convective currents in the fluid, describes the charge relaxation phenomena in the moving liquid. The charge received by the droplets during acceleration by an external electric pulse is an important parameter influencing dynamics of droplets in the pressure chamber. The model is illustrated with simulations of detachment of high conductivity acetone droplets and low conductivity n-pentane droplets.

## 1 INTRODUCTION

The application of strong electric fields on liquids is used in many engineering applications to induce liquid atomization in a controlled manner. In electrosprays [1, 2], the droplet size and the opening angle of the spray cone can be affected by charging the liquid

prior to its atomization. In electrically driven on-demand droplet generators, millimetric droplets pending from a capillary can be detached on a controlled manner by applying strong electrical pulses. The method provides reliable injection of liquid samples in the experimental chamber, at a broad range of atmospheric conditions [3].

Deformations of the phase boundary induced by electric fields result in changes in the electric field and force distribution. The mechanical and electric problems are thus strongly coupled. Additionally, due to the presence of intrinsic ionic species and dissolved impurities, liquids exhibit some electrical conductivity associated with charge migration. Dynamic charging effects in liquid droplets and convection of free charge can strongly alter liquid motion. Moreover, the accumulation of free charge in droplets can result in the generation of charged droplets from initially uncharged liquid. This behavior requires an electroquasistatic field representation, taking into account both conduction and displacement electric currents in the liquid.

We discuss a conduction-convection model for the simulation of droplet dynamics under the influence of electric fields. The liquid interface is captured using the Volume of Fluid method , allowing for an efficient representation of topology changes in the phase boundaries. The electric problem is solved using the resulting diffuse interface, and the resulting electric force is introduced as a source term for the hydrodynamic problem. Wetting is taken into account by using a dynamic contact angle model.

The numerical study of liquid droplets generation in an on-demand droplet generator [3] is considered in this work. Detachment dynamics of acetone and n-pentane droplets, exhibiting respectively high and low conductivity, are reproduced numerically, and illustrate the effect of conductivity on electrically induced droplet motion.

## 2 GOVERNING EQUATIONS

### 2.1 The Fluid Flow Problem

In this paper, we focus on the application of an external electric pulse to drive droplet detachment. As a result, we restrict the study of the generator to the lower range of temperatures, where droplet injection does not involve phase transitions. Under these atmospheric conditions, the fluid flow problem is governed by the incompressible Navier-Stokes equations:

$$\frac{\partial \rho \vec{u}}{\partial t} + \nabla \cdot \rho \vec{u}\vec{u} = -\nabla p + \nabla \cdot \left(\mu \left[\nabla \vec{u} + \nabla \vec{u}^{\mathrm{T}}\right]\right) + \rho \vec{g} + \vec{f_{\mathrm{s}}} + \vec{f_{\mathrm{e}}}\,, \tag{1}$$

$$\nabla \cdot \vec{u} = 0\,, \tag{2}$$

where $\vec{u}$ denotes fluid velocity, $\rho$ is the density, $\mu$ the dynamic viscosity and $p$ the pressure. The driving terms $\vec{f_{\mathrm{s}}}$ and $\vec{f_{\mathrm{e}}}$ are, respectively, the surface tension force density acting at the interface between the two fluid phases, and the electric force density. The former is related to the phase boundary properties according to Young-Laplace equation,

$$\vec{f_s} = 2\gamma H \vec{n}\,, \tag{3}$$

where $\gamma$ is the surface tension characterizing the fluid-fluid interface, $H$ is the mean curvature and $\vec{n}$ the interface normal.

This surface tension contribution needs also to be considered at contact lines, where the fluid-fluid interface meets solid walls. This is particularly important in the case of this droplet generator, since wetting of the surface of the capillary by test fluids strongly affects the detachment process [4]. The contact line problem is described in terms of a local apparent contact angle, $\theta$. For static contact lines, this angle is limited by a minimal advancing and maximal receding values, $\theta_{adv}$ and $\theta_{rec}$, respectively [5]. Those values can be determined experimentally. In dynamic cases, the apparent contact angle value depends on the local contact line velocity, $u_{\mathrm{cl}}$, additionally. In this work, the dynamic contact angle is calculated from the Kistler correlation [6]:

$$\theta = f_{\mathrm{H}}\left(C_a + f_{\mathrm{H}}^{-1}\left(\theta_{\mathrm{adv/rec}}\right)\right)\,, \tag{4}$$

$$\text{with} \quad f_{\mathrm{H}}\left(x\right) = \arccos\left(1 - 2\tanh\left[5.16(\frac{x}{1+1.31x^{0.99}})^{0.706}\right]\right)\,. \tag{5}$$

In (4), the capillary number $\mathrm{Ca} = \frac{\mu_{\mathrm{liquid}}\cdot u_{\mathrm{cl}}}{\gamma}$ is a signed quantity, taken positive for an advancing contact line, negative otherwise.

### 2.2 The Electric Field Problem

In electrically conductive fluids, the current density, $\vec{J}$, is composed of a conductive and a conductive components:

$$\vec{J} = \rho_e\vec{u} + \kappa\vec{E}\,, \tag{6}$$

where $\kappa$ is the ohmic conductivity of the fluid and $\rho_e$ the charge density associated with the free charge carriers in the fluid. Using the free charge continuity equation,

$$\frac{\partial\rho_e}{\partial t} + \nabla\cdot\vec{J} = 0\,, \tag{7}$$

and introducing an electric potential so that $\vec{E} = -\nabla\Phi$ yields the equations describing the electric problem:

$$\nabla\cdot\varepsilon\nabla\Phi = -\rho_e\,, \tag{8}$$

$$\frac{\partial\rho_e}{\partial t} + \nabla\cdot(\rho_e\vec{u}) = \nabla\cdot\kappa\nabla\Phi\,, \tag{9}$$

where $\varepsilon$ is the permittivity of the media.

The electric force density applied on the fluid can be obtained from the electric field distribution using the Maxwell stress tensor:

$$\vec{f_{\mathrm{e}}} = \nabla\cdot\left(\varepsilon\vec{E}\otimes\vec{E} - \frac{1}{2}\varepsilon E^2\vec{\vec{I}}\right)\,. \tag{10}$$

## 3 NUMERICAL APPROACH

The electrohydrodynamic problem involves two different fluids, for which a description of the interface is required. We use the Volume of Fluid (VoF) method [7], a diffuse interface approach, to describe the topology of the fluid-fluid interface. The solution to Eq. (1)-(5) and (8)-(10), modeling the coupled problem is implemented, along with the VoF method, using the OpenFOAM [8] framework, as described in detail below.

### 3.1 Solution of the Fluid Flow Problem

In the Volume of Fluid method, the fluid material properties are represented using the volume fraction, $\alpha$, of one of the fluids in each cell of the computational grid. The Navier-Stokes equations are solved assuming a single phase whose local material properties are calculated from the volume fraction. The interface is advanced in time by transporting the volume fraction:

$$\frac{\partial \alpha}{\partial t} + \nabla \cdot (\alpha \vec{u}^*) = 0\,, \tag{11}$$

with $\alpha \in [0,1]$. In Eq. (11), $\vec{u}^*$ is a modified velocity field, including an optional numerical compression velocity pointing normal to the interface [9]. The effective fluid properties at the interface between fluid 1 and fluid 2 are determined by weighted averaging as

$$\rho = \alpha \cdot \rho_1 + (1-\alpha) \cdot \rho_2\,, \tag{12}$$

$$\mu = \alpha \cdot \mu_1 + (1-\alpha) \cdot \mu_2\,. \tag{13}$$

The evolution of the volume fraction does not require interface reconstruction, so that topology changes of the phase boundary are implicitly taken into account.

The surface tension force applied on the diffuse interface can be described using the volume fraction, as a body force [10]:

$$\vec{f}_\mathrm{s} = -\gamma \nabla \cdot \left( \frac{\nabla \alpha}{||\nabla \alpha||} \right) \nabla \alpha\,. \tag{14}$$

The contact angle model (4) provides the necessary boundary condition for the computation of the contribution of the surface tension at the contact line. The velocity of the contact line is evaluated, according to the scheme proposed in [5], as

$$u_\mathrm{cl} = \frac{\vec{u}_\mathrm{w} \cdot \vec{n}_\mathrm{i}}{\sqrt{1 - (\vec{n}_\mathrm{w} \cdot \vec{n}_\mathrm{i})^2}}\,, \tag{15}$$

where $\vec{u}_\mathrm{w}$ is the fluid velocity near the solid wall, $\vec{n}_\mathrm{w}$ is the normal vector to the wall and $\vec{n}_\mathrm{i} = \nabla\alpha / ||\nabla\alpha||$ is the normal to the phase boundary interface.

The pressure-velocity equations (1), (2) are solved numerically using the PISO algorithm as implemented, e.g., in the INTERFOAM solver (see [11]). As the electric force density driving fluid motion depends on the fluid velocity through the convection term of the charge conservation equation (9), we apply a fixed-point iteration between the electric field solver and the fluid flow solver at every time step of the simulation.

### 3.2 Solution of the Electric Field Problem

Sharp interface representations for the material boundaries are usually used in pure electric field computations. Methods based on interface tracking using a moving mesh can be readily applied for droplet simulations [12], as long as topology changes are not involved. The motion of liquids in this work involves strong stretching as well as splitting of the fluid-fluid interface. Sharp interface tracking via a moving mesh would therefore require explicit treatment of interface topology changes, as in e.g. [13]. As droplet detachment from a capillary involves multiple topology changes from the liquid thread and secondary droplets [14], such a treatment would need to be applied frequently. We therefore adopt a VoF-like method for the solution of the electric field equations (9), (10).

The electric field problem is solved on the same computational grid as the fluid problem using averaged electric properties, defined similarly to Eq. (12) and (13):

$$\frac{1}{\varepsilon} = \frac{\alpha}{\varepsilon_1} + \frac{1-\alpha}{\varepsilon_2}\,, \tag{16}$$

$$\frac{1}{\kappa} = \frac{\alpha}{\kappa_1} + \frac{1-\alpha}{\kappa_2}\,. \tag{17}$$

Note that in (16) and (17), harmonic averaging of the material properties is used rather than arithmetic averaging. This relates to the particular form of the expected field solution, where the electric field is essentially normal to the phase boundary for conductive liquids. In that case, harmonic averaging leads to more accurate results than arithmetic averaging [15, 16].

Equations (9), (10) are updated by a time staggering scheme as

$$\nabla \cdot \varepsilon^{n+1/2} \nabla \Phi^{n+1/2} = -\rho_{\mathrm{e}}^{n+1/2}\,, \tag{18}$$

$$\frac{\rho_{\mathrm{e}}^{n+1} - \rho_{\mathrm{e}}^{n}}{\Delta t} + \nabla \cdot (\rho_{\mathrm{e}}^{n+1/2} \vec{u}^{n+1/2}) = \nabla \cdot \kappa^{n+1/2} \nabla \Phi^{n+1/2}\,. \tag{19}$$

The charge density, $\rho_{\mathrm{e}}^{n+1/2}$ in (18), is initially unknown. Thus, an inner fixed-point iteration is applied for the solution of (18), (19) in addition to the outer iteration loop which is applied in every time step of the simulation.

## 4 Validation Example

In order to validate the numerical approach, a simple one-dimensional example is considered, see Fig. 1. A planar liquid layer of thickness $L_l$ is transported passively with a constant velocity $u$ in a surrounding gaseous environment. The two fluids are characterized by the permittivities, $\varepsilon_l$ and $\varepsilon_g$, and electric conductivities, $\kappa_l$ and $\kappa_g$, respectively. At time $t_0 = 0$, an electric voltage $U$ is applied between the two boundaries of the computational domain. When the external voltage is switched on, electric charges start accumulating at the front and back interfaces of the liquid layer. The induced charge moves together with the phase boundaries and keeps increasing until a steady state is

reached. The analytic solutions for the transient electric field and surface charge densities are given by

$$E_{\{l,g\}} = \frac{U}{L} \cdot \left[ \frac{\kappa_{\{g,l\}}}{\kappa_*} \cdot \left(1 - \exp^{-\frac{\kappa_*}{\varepsilon_*} t}\right) + \frac{\varepsilon_{\{g,l\}}}{\varepsilon_*} \cdot \exp^{-\frac{\kappa_*}{\varepsilon_*} t} \right], \tag{20}$$

$$\sigma_{\pm} = \pm \frac{U}{L} \cdot \frac{\varepsilon_g \kappa_l - \varepsilon_l \kappa_g}{\kappa_*} \cdot \left(1 - \exp^{-\frac{\kappa_*}{\varepsilon_*} t}\right) \tag{21}$$

where $E_l$ and $E_g$ are the electric field strengths in the liquid and gas layers, respectively, $\sigma_{\pm}$ are the two interface charge densities, $\varepsilon_* = (L_g \varepsilon_l + L_l \varepsilon_g)/L$, $\kappa_* = (L_g \kappa_l + L_l \kappa_g)/L$ and $L = L_l + L_g$ is the total length of the computational domain. Note that this solution does not depend on fluid velocity.

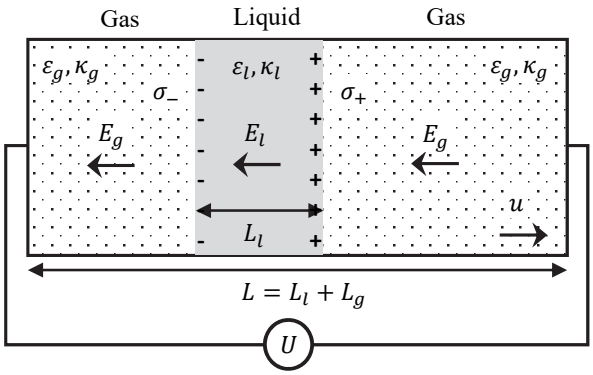


**Figure 1**: Schematic representation of the moving layer problem.

Figure 2 shows the results of the numerical simulation compared to the analytic solution. The parameters of the problem are chosen as: $u = 1\,\mathrm{m\,s^{-1}}$, $\varepsilon_l = 4 \cdot \varepsilon_0$, $\varepsilon_g = 1 \cdot \varepsilon_0$, $\kappa_l = 1.5 \times 10^{-8}\,\mathrm{S\,m^{-1}}$ and $\kappa_g = 1 \times 10^{-12}\,\mathrm{S\,m^{-1}}$. As seen in the figure, a good agreement between the analytic and numerical results is obtained even for the coarse grid used here. Similarly to the numerical solution for the fluid density, the electric field distribution at the phase boundaries is subject to numerical diffusion. However, the computed total interface charge agrees nearly perfectly with the analytic solution.

## 5 Droplet Generator Simulations

The model described in the previous section is applied in the simulation of an electrically driven droplet generator [3]. The generator setup is shown in Fig. 3. A metallic capillary tube, kept at ground potential, introduces liquid in the pressure chamber. Two electrodes on each sides of the capillary are connected to a high-voltage source. In order to prevent electric breakdown in the test chamber, the electrodes are embedded in two insulator blocks. The chamber is capable of sustaining a high-pressure and high-temperature environment. The liquid introduced from the capillary can be heated separately. In the

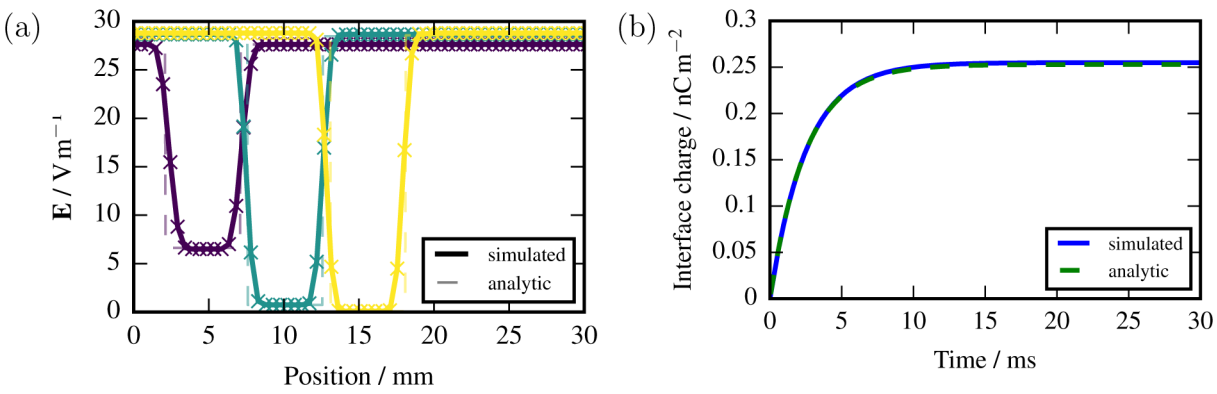


**Figure 2**: Comparison between analytic and numerical results for the moving liquid layer. (a) Electric field distribution at three different time instants after the external voltage is switched on. (b) Magnitude of the total charge at either fluid interface as a function of time.

simulations and experiments detailed below, the liquid is introduced at the same temperature as the surrounding gaseous environment.

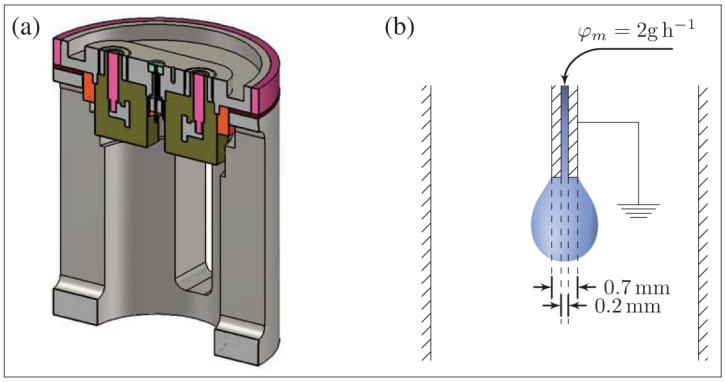


**Figure 3**: (a) Full model of the droplet generator including capillary, electrodes and test chamber (cf. [3]). (b) Schematic view and main parameters of the simulation model.

Liquid is introduced into the capillary at a constant mass flow rate of $2\,\mathrm{g\,h^{-1}}$, in the absence of electric fields, until a pendant droplet forms at its end.Typical filling times for a single droplet are in the range of 2 s to 6 s, yielding droplet volumes in the range 2 µL to 5 µL, depending on the atmospheric conditions in the chamber and initial liquid temperature. Due to the wettability of the capillary, the droplet wets the sides of the capillary and is held in place by surface tension. As the droplet size increases, the equilibrium between the weight of the droplet and its surface tension leads to slow dewetting of the sides of the capillary. An optical setup monitoring droplet presence then triggers the detachment process. The mass flow is interrupted to prevent from generating additional droplets, while the electric voltage is switched on. Typical electric pulses apply a peak voltage of 1 kV to 5 kV over a duration of 10 ms to 40 ms. The electric forces applied

on the droplet accelerate the droplet for the duration of the pulse, eventually leading to droplet detachment.

Experimental observations show that the dynamics of the flow induced by the electric field strongly depend on the electrical properties of the test liquid. The two cases are analyzed separately in the following sections, in order to emphasize the different charging and fluid flow dynamics.

Although the geometry of the droplet is not axisymmetric, the electric field distribution is nearly so in the vicinity of the capillary. In order to reduce the computational cost of simulations, a 2D axisymmetric approach is therefore used in what follows.

Simulations are performed with a grid resolution of $\frac{1}{\delta x} = 2.5 \times 10^{-5}\,\mathrm{m}^{-1}$, corresponding to approximately 35 cells per primary droplet radius. This resolution is chosen as further refinement of the grid does not influence the dynamics of primary droplets, while still capturing the qualitative behavior of the liquid thread and secondary droplets. The time step size is chosen as $\Delta t = 2\,\mu\mathrm{s}$ for this grid size, according to the stability limit for surface tension driven flow [17].

In order to save computational effort, the initial filling regime is simulated on a reduced domain centered on the capillary. The computational domain is extended vertically for simulating droplet detachment events. The two domains have, respectively, 20960 and 50200 cells for the chosen resolution. The typical time required to simulate the droplet filling is 24 h; the typical time required for simulating droplet detachment is 8 h.

### 5.1 Acetone Droplet Generation

At 1 bar, 293 K, the electrical conductivity of acetone is $\kappa = 20\,\mu\mathrm{S}$ and its relative permittivity $\varepsilon_\mathrm{r} = 21$. The resulting free charge relaxation time is therefore of the order of 10 µs, orders of magnitude smaller than the voltage pulse duration, $\tau_p \approx 10\,\mathrm{ms}$ and the time scale of fluid motion. Acetone can be therefore considered as highly conductive for the considered experimental conditions. The result of the simulation is shown in Fig. 4. The voltage profile assumed for the simulation, peaks at 2 kV, over a duration of 11.5 ms.

The droplet is initially pulled downwards during the short electric pulse. After the end of the pulse, the droplet continues stretching under its own inertia, eventually leading to detachment. A comparison of the dynamics of the droplet detachment, Fig. 4, at different time instants before and after detachment, shows a close agreement between simulated and experimental dynamics. A slight discrepancy is visible in the form of a secondary droplet, originating from the liquid thread at the time of detachment, that follows the primary droplet in the experiment.

A detailed investigation of the dynamics of detachment is shown in Fig. 5. The volume of the detached primary droplet, illustrated in Fig. 5b is weakly dependent on the applied voltage, varying less 3% in the investigated range of voltages, 2-5kV. The detachment time, illustrated in Fig. 5a, is however strongly dependent on the generator voltage. At lower voltages, a fast variation of the detachment time is observed, while at higher voltages, the detachment time decreases nearly linearly with increasing applied voltage.

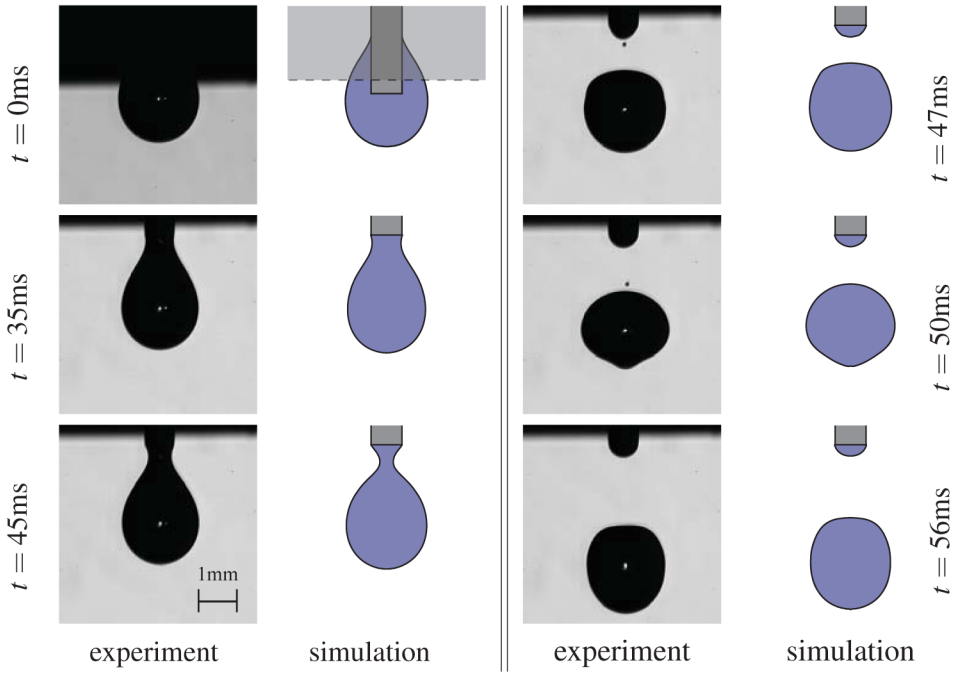


**Figure 4**: Acetone droplet dynamics: comparison between simulation and experiment for the droplet shape in the generator at different time instants during the detachment process. The experimental images were obtained using a high speed shadowgraphy imaging technique as described in [3].

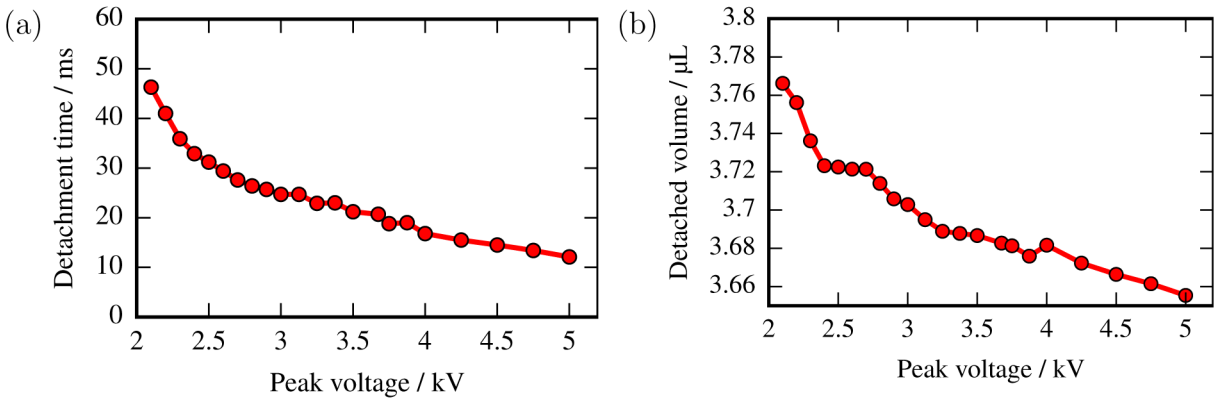


**Figure 5**: Detachment characteristics vs. applied voltage for acetone droplets. (a) Detachment time and (b) droplet volume vs. generator voltage.

## 5.2 n-Pentane Droplet Generation

At 1 bar, 293 K, the relative permittivity of n-pentane is $\varepsilon_r = 1.84$. In the absence of impurities, its electrical conductivity is in the range of $\kappa = 20\,\mathrm{pS\,m^{-1}}$. The resulting free charge relaxation time is therefore of the order of 1 s, which is much longer than the applied voltage pulse duration. As a result, the amount of dynamic charging resulting

from the external electric pulse is low, so that electric fields penetrate the droplet. The effective polarization forces initial push the droplet upwards, causing it to ascend on the capillary. The weight of the droplet, unbalanced after the end of the electric pulse, results in the droplet accelerating downwards, eventually leading to detachment.

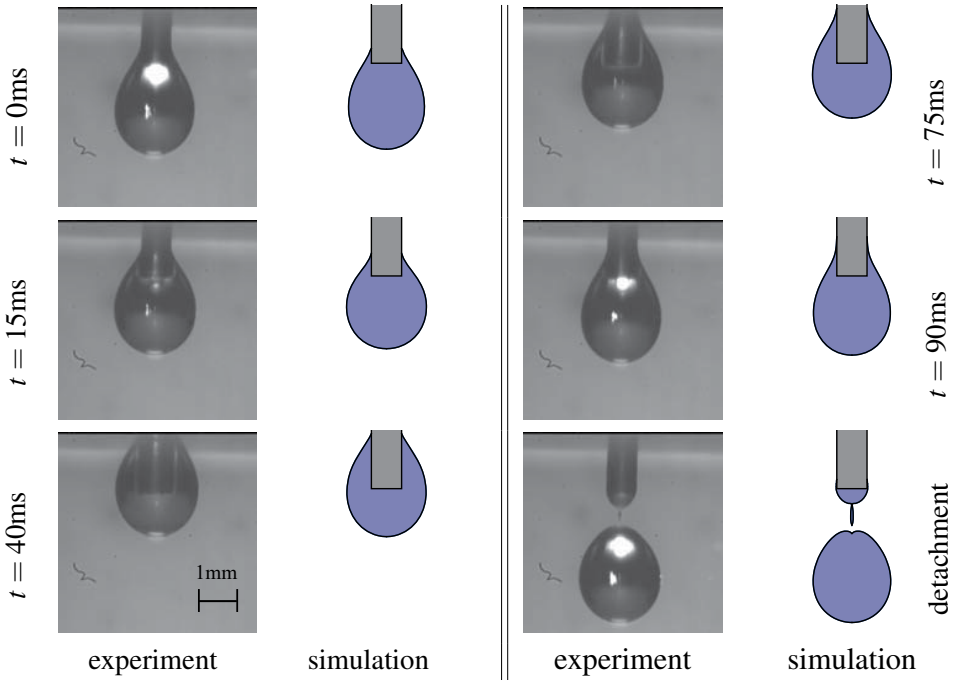


**Figure 6**: n-pentane droplet dynamics: comparison between simulation and experiment for the droplet shape in the generator at different time instants during the detachment process.

Unlike the case of acetone droplet generation, in the absence of shielding of the capillary by charged conductive liquid, the electric field distribution strongly depends on the location of the droplet on the capillary. The dependency of the detachment time on the applied voltage is thus much lower than in the case of conductive droplets, see Fig. 7a. A small charge is carried by the droplet, after detachment, due to the long relaxation time in n-pentane, as seen in Fig 7b.

## 6 Conclusion

The proposed electrohydrodynamic simulation approach allows for accurate modeling of droplet dynamics under the influence of strong electric fields. In particular, it takes into account conductive, capacitive as well as convective electrical currents in the fluid. These contributions determine the induced electric charge in the droplet before and after detachment and, therefore, are crucial for the droplet dynamics. Simulation results are shown for an electrically driven droplet generator using highly conductive acetone droplets and low conductivity n-pentane droplets, respectively. In both cases, excellent

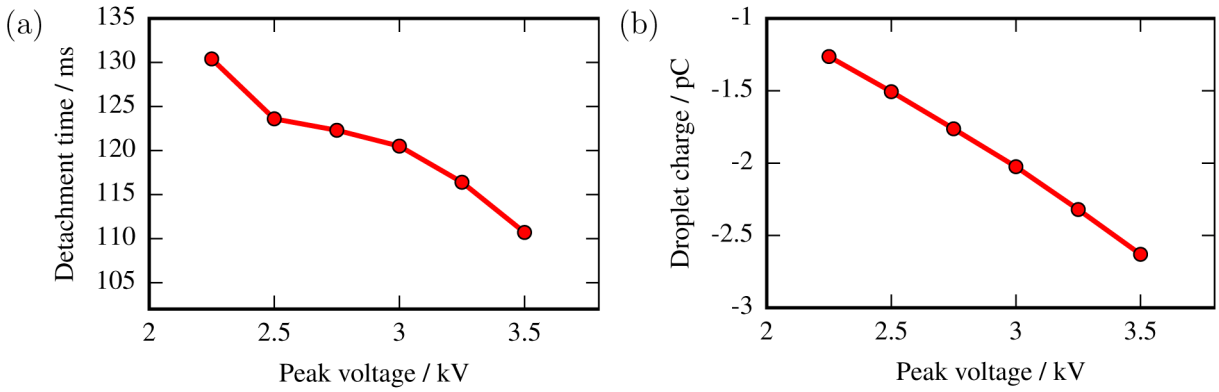


**Figure 7**: n-pentane droplet characteristics vs. generator voltage. (a) Detachment time and (b) droplet charge after detachment.

agreement with the measurements is found. The droplet charging effect is demonstrated for n-pentane droplets as well as for acetone droplets under long voltage pulses. This investigation shows that due to the very different relaxation times, the charging behavior of the two liquids is very different. This behavior is, furthermore, closely related to the droplet dynamics in the generator. In particular, we demonstrate that due to their electric properties, the detachment mechanisms for acetone and n-pentane droplets are completely different. For low conductivity (n-pentane) droplets, the detachment is primarily due to the uncompensated droplet weight, which dominates droplet dynamics only after the generator voltage is switched off.

## ACKNOWLEDGEMENT

This work was funded by the German Research Foundation (DFG) within the Collaborative Research Centre SFB-TRR 75 "Droplet Dynamics Under Extreme Ambient Conditions".

## References

[1] M. Cloupeau and B. Prunet-Foch. Electrohydrodynamic spraying functioning modes: a critical review. *J. Aerosol Sci.*, 25(6):1021 – 1036, 1994.

[2] A. Jaworek and A. Krupa. Classification of the modes of ehd spraying. *J. Aerosol Sci.*, 30(7):873 – 893, 1999.

[3] F. Weckenmann, B. Bork, E. Oldenhof, G. Lamanna, B. Weigand, B. Boehm, and A. Dreizler. Single acetone droplets at supercritical pressure: Droplet generation and characterization of PLIFP. *Z. Phys. Chem.*, 225:1417–1431, 2011.

[4] B. Chang, G. Nave, and S. Jung. Drop formation from a wettable nozzle. *Commun. Nonlinear Sci.*, 17(5):2045 – 2051, 2012.

[5] I. V. Roisman, L. Opfer, C. Tropea, M. Raessi, J. Mostaghimi, and S. Chandra. Drop impact onto a dry surface: Role of the dynamic contact angle. *Colloids and Surfaces A: Physicochemical and Engineering Aspects*, 322(13):183 – 191, 2008.

[6] S. F. Kistler. Hydrodynamics of wetting. *Wettability*, 6:311–430, 1993.

[7] C. W. Hirt and B. D. Nichols. Volume of fluid (VOF) method for the dynamics of free boundaries. *J. Comput. Phys.*, 39(1):201 – 225, 1981.

[8] Openfoam. openfoam.org.

[9] H. G. Weller. A new approach to VOF-based interface capturing methods for incompressible and compressible flow. *OpenCFD Ltd., Report TR/HGW/04*, 2008.

[10] J. U. Brackbill, D. B. Kothe, and C. Zemach. A continuum method for modeling surface tension. *J. Computat. Phys.*, 100(2):335 – 354, 1992.

[11] H. Rusche. *Computational fluid dynamics of dispersed two-phase flows at high phase fractions*. PhD thesis, Imperial College London, 2003.

[12] H. Songoro. *Electrohydrodynamic Modeling of Droplet Vibrations under the Influence of Electric Fields*. PhD thesis, Technische Universität, Darmstadt, 2015.

[13] S. Quan and D. P. Schmidt. A moving mesh interface tracking method for 3d incompressible two-phase flows. *J. Comput. Phys.*, 221(2):761 – 780, 2007.

[14] X. Zhang and O. A. Basaran. Dynamics of drop formation from a capillary in the presence of an electric field. *J. Fluid Mech.*, 326:239–263, 11 1996.

[15] G. Tomar, D. Gerlach, G. Biswas, N. Alleborn, A. Sharma, F. Durst, S.W.J. Welch, and A. Delgado. Two-phase electrohydrodynamic simulations using a volume-of-fluid approach. *J. Comput. Phys.*, 227(2):1267 – 1285, 2007.

[16] W. Rohlfs, G. F. Dietze, H. D. Haustein, and R. Kneer. Two-phase electrohydrodynamic simulations using a volume-of-fluid approach: A comment. *J. Comput. Phys.*, 231(12):4454 – 4463, 2012.

[17] C. Galusinski and P. Vigneaux. On stability condition for bifluid flows with surface tension: Application to microfluidics. *J. Comput. Phys.*, 227(12):6140 – 6164, 2008.